Micro-Electrical Impedance Spectroscopy and Identification of Patient-Derived, Dissociated Tumor Cells

Salil P. Desai, Anthony Coston, and Andrew Berlin

***Abstract*— Fine needle aspirate sampling of tumors requires acquisition of sufficient cells to complete a diagnosis. Aspirates through such fine needles are typically composed of small cell clusters in suspension, making them readily amenable to microfluidic analysis. Here we show a microfluidic device with integrated electrodes capable of interrogating and identifying cellular components in a patient-derived sample of dissociated tumor cells using micro-electrical impedance spectroscopy (μEIS). We show that the μEIS system can distinguish dissociated tumor cells in a sample consisting of red blood cell (RBCs) and peripheral blood mononucleated cells (PBMCs). Our μEIS system can also distinguish dissociated tumor cells from normal cells and we show results for five major cancer types, specifically, lung, thyroid, breast, ovarian, and kidney cancer. Moreover, our μEIS system can make these distinctions in a label-free manner, thereby opening the possibility of integration into standard clinical workflows at the point of care.**

***Index Terms*— Fine needle aspiration biopsy, electrical impedance spectroscopy, fine needle aspirate (FNA), single cell analysis, microfluidic flow cytometry, label-free detection, cell enumeration, patient-derived cells.**

I. Introduction

DIAGNOSTIC workflows in oncology are underpinned by the need to acquire sufficient cells via biopsy, and to determine which cells in the acquired biopsy are malignant. Thus, the problem generalizes to the acquisition of cellular samples and subsequent enumeration and classification of these cellular samples. Fine needle aspirates [1], [2] represent one such class of samples which are used in the clinic for breast, lung and thyroid nodule biopsies. By nature of their acquisition, fine needle aspirates (FNAs) are small aggregates of cells as compared to core needle biopsies, requiring less sample preparation overhead for microfluidic analysis. While FNAs open considerable opportunities for tumor diagnosis and simpler clinical workflows, technical challenges remain – primary among them, the robust and reliable acquisition of sufficient cells for diagnostic purposes [3]–[5]. Surgical pathologists are typically unaware of how many cells have been collected, whether those cells are the suspicious cells that are the target of the biopsy, and whether the sample is indeed sufficient for downstream pathological and genetic analysis. Moreover, it remains unclear if the collected cells are indeed relevant for diagnosis [3].

We aim to address both the challenges of enumeration and classification using our μEIS system. The μEIS system has both the capability to count cells in a label-free manner and to distinguish the types of cells in the acquired sample. As biopsy sample analysis increasingly shifts towards molecular, rather than multi-cellular morphological methods, we envision that a combination of machine learning techniques for signature recognition of suspicious cells, coupled with downstream molecular analysis, will enable the μEIS system to characterize a wide-range of patient-derived FNAs for precise, personalized cancer diagnosis at the point of care. Rapid sample characterization at the point of care has the potential to reduce the number of biopsy samples that must be acquired, thereby reducing anesthesia duration and potential complications such as bleeding, as well as reducing the burden of return visits to repeat biopsy procedures that failed to attain samples having sufficient cellularity.

For demonstration purposes, we show the application of the μEIS to the discrimination of patient-derived cancer cells acquired from dissociated human samples. The analysis of these dissociated samples serves as an important proof-of-concept and validation of the use of μEIS on patient samples. We envision the μEIS can quickly be integrated into clinical workflows as a rapid desktop analysis device at the point of care, and could potentially be directly integrated into tumor sampling needles or syringes.

II. Materials and Methods

A. A. Device Design

Fabricated devices, pictured in Figure 1, include dual inputs for analyte as well as a physiological buffer solution, a sample preparation stage that removes debris and tissue aggregates, a hydrodynamic focusing stage that positions the analyte for analysis, and a series of multi-electrode analysis stages that perform electrical impedance spectroscopy. Capability for external optical detection of cells transiting the electrical detectors is also provided for sensor validation purposes. Channels were designed to accommodate multiple cells and narrow to single cell streams in the 25-micron wide and 25-micron tall detection region, as shown in the inset to Figure 1. The cell interrogation region consists of two

Manuscript received August 30, 2018; accepted September 20, 2018. Date of publication June 4, 2019; date of current version June 28, 2019. This work was supported by the Draper Laboratory. This paper was presented in part at the EMBS Micro and Nanotechnology in Medicine Conference, Kauai, HI, USA, December 10–14, 2018. *(Corresponding author:* Andrew Berlin.)

S. P. Desai is with Phenomyx LLC, Cambridge, MA 02139 USA (e-mail: salil@phenomyx.com).

A. Coston and A. Berlin are with the Draper Laboratory, Cambridge, MA 02139 USA (e-mail: anthony.coston@sloan.mit.edu; aab@alum.mit.edu).

Digital Object Identifier 10.1109/TNB.2019.2920743

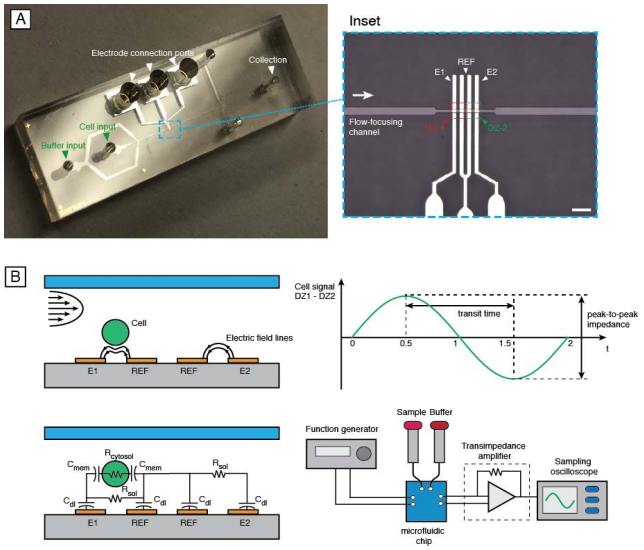

Fig. 1. *Microelectrical Impedance spectroscopy (μEIS) system on chip. (A) Micrograph of a microfabricated chip showing buffer and cell inputs to focus a single stream of cells through the detection region. Right panel shows the dashed blue region inset, a magnified image of the eletrode region with dual electrode pairs for detection and time-of-flight analysis. Electrodes are labeled E1and E2 and precision-aligned to the detection channel. Flow-focusing channels narrow to the detection region to ensure streams of single cells. Scale bar 50 micron. (B) Cross-sectional schematic of the detection channel (not-to-scale) showing a particle passing over two electrode pairs (E1 and E2). The impedance signal is measured differentially as ZE1 - ZE2. Hydrodynamic focusing is used to center the cell in the flow channel. Right panel shows a schematic view of the impedance signal. When the distance between the two measurement areas and time separating the signal peaks are known, the speed of the particle can be calculated. The non-occupied electrode can serve as an important control and determine noise floors for the measurement.*

electrode pairs in distinct detection zones labeled DZ1 and DZ2 in Figure 1A.

Devices were designed using AutoCAD software and fabricated using standard soft lithography techniques [6] Briefly, the process consists of building microfluidic masters with multiple layers of SU-8 of 25- and 50-micron thickness. The specific SU-8 layer defines the microfluidic channels which are molded using standard soft lithographic techniques. Both electrical and fluidic connections are made through biopsy-punched holes made prior to bonding to a diced Pyrex wafer with patterned electrodes. Electrodes are fabricated with electron-beam evaporated gold films patterned with standard lift-off techniques. A titanium oxide layer deposited on the gold (and removed from any channel-exposed regions) facilitates bonding to the PDMS fluidic chip.

B. Electrical Impedance Spectroscopy Setup

The electrical detection system is shown in Figure 1B. The cross-sectional schematic of the detection channel (not-to-scale) of the microchannel shows a particle passing over two electrode pairs (E1 and E2). The particle is hydrodynamically focused in the center of the flow channel. The impedance signal across these two electrode pairs is measured differentially as DZ1 - DZ2, when the electrodes are excited at frequency of 250 kHz. The resulting impedance signal (Figure 1B, right panel) is schematically depicted, tracing the trajectory of a single particle – when the distance between the two measurement areas and time separating the signal peaks are known, the speed of the particle can be calculated. The non-occupied electrode can serve as an important control and determines noise floors for the measurement. The two measurements of peak-to-peak amplitude and transit time are important metrics for distinguishing the cells in the μEIS system. The equivalent circuit model for a cell traversing the electrodes is depicted in Figure 1B (bottom panel). At the frequencies of interest, the membrane capacitance is negligible and the electric field can probe the cytosolic resistance of the cell (which is in turn proportional to its volume) and make sensitive measurements of cell size and morphology differences amongst cells. The μEIS system setup is schematically depicted in Figure 1B (bottom panel) where cells and buffer are passed through the detection region using precise pressure-control. The electrodes are energized by a function generator and the electrical signals are amplified by a custom-built transimpedance amplification circuit. Amplified signals are viewed in real-time and recorded using a sampling oscilloscope. Stored waveforms are further analyzed using statistical data analysis techniques.

C. Dissociated Tumor Cells and Cell Culture

Dissociated tumor cells (DTCs) were acquired directly from Conversant Bio (Huntsville, AL) for a range of indications and cancer stages. Matched peripheral blood mononuclear (PBMCs) cells for specific DTCs were also acquired from Conversant Bio. These DTCs were both mechanically and enzymatically dissociated and provided in frozen sample vials. DTCs were stored frozen (at -170 °C) and thawed 24 hours prior to experiments. DTCs were maintained in standard serum-supplemented cell culture media prior to experiments and washed 3X in PBS before injecting in to the μEIS microfluidic chip. Normal target organ cell cultures, specifically, thyroid, breast, lung, and ovarian cells were acquired from ATCC (Arlington, VA) and maintained in a 5% CO_2 environment at 37 °C and cultured in media using standard protocols.

III. Results

A. Real-Time Impedance Measurement

Impedance measurements can be made in real-time using our μEIS setup. Current through the detection zones is converted to a voltage through a sensitive transimpedance amplifier, so |Z| is proportional to |V|. As described in Figure 1B, for a cell passing through the electrode region, at the excitation frequencies used (between 200 kHz and 250 kHz), the electrode double-layer capacitance and membrane capacitance can effectively be considered shorts and the field will be modulated by the cytosolic resistance ($R_{cytosol}$). The resulting current through the buffer medium and the cell is proportional to the cell size.

By adjusting the flow rates and cell concentration, we can ensure that a single cell passes through each detection region (as shown in stop-action images in Figure 2A) and we can use the differential signal as the cell passes through the first electrode region and then the second. The difference in the signals of a cell passing through the electrodes provides a strong signal-to-noise ratio. Importantly, the non-occupied electrode can serve as an important control and determine noise floors for the measurement. The peak-to-peak voltage

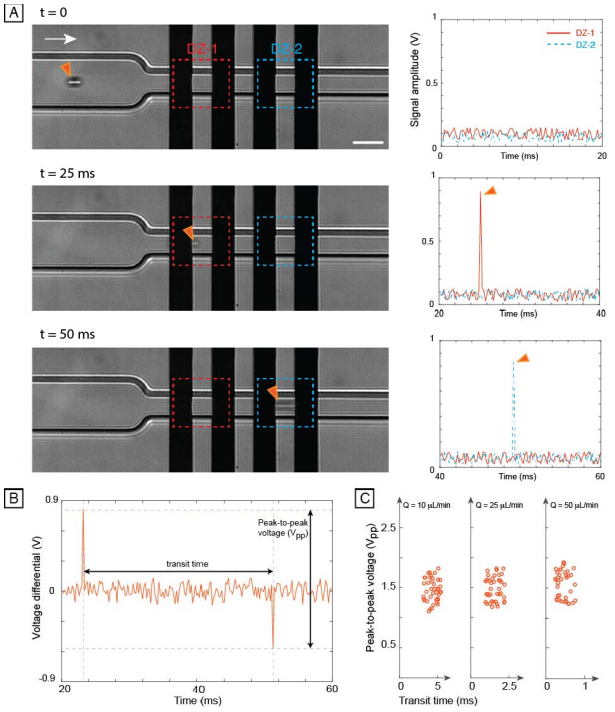

Fig. 2. *Real-time measurements of live cells. (A) Left panel shows stop action images of a single cancer cell entering the detection region (t = 0ms) and then the two subsequent time points when the cell is in each detection zone, DZ1 (25 ms later) and then DZ2 (50 ms later). Scale bar 25 micron. Right panel shows voltage traces captured from the transimpedance amplifier (where $|V|$ is proportional to $|Z|$ impedance change). (B) The differential voltage measurement between the electrodes yields a measure of the cell position, size and transit time through the detection region. (C) Scatter plots of differential voltage against transit times show that individual cells (n = 25) can be reliably discriminated at lower flow rates. As flow rates increase, the system approaches its maximum detection rate, limited by confounding of signals from adjacent cells as the electrical measurements do not have time to settle between cell encounters.*

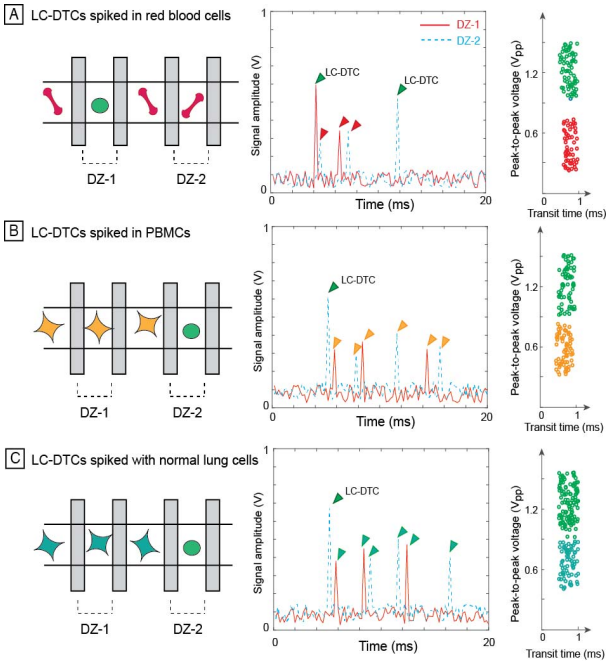

Fig. 3. *Real-time measurements of dual cell populations. (A) Lung cancer dissociated tumor cells (LC-DTCs) are spiked in a red blood cell (RBC) suspension. Left panel shows schematic of cells passing through the two detection zones and the corresponding captured voltage traces. Right panel shows overlays of peak-to-peak voltages, showing discriminations between the two cell types (LC-DTCs, green circles, RBCs, red circles, n = 50 for each population). Flow rate Q = 50 Lmin (B) LC-DTCs spiked in peripheral blood mononucleated cell samples. Voltage traces and peak-to-peak voltages show that the cells can be effectively discriminated, n = 50 and Q = 50 Lmin. (C) LC-DTCs mixed with normal lung cells, show that even with similar cell types, cancer cells can be effectively discriminated with peak-to-peak voltage measurements, n = 50 and Q = 50 Lmin.*

differential (V_{pp}) and transit time ($t_{transit}$), as plotted in Figure 2B, are important metrics for detecting individual cells in our μEIS setup. Moreover, these measurements can be made at a range of flow-rates, as shown in Figure 3C, where scatter plots of V_{pp} versus $t_{transit}$ show that consistent identifications can be made at flow rates up to 50 μL/min.

B. Real-Time Impedance Measurements of DTCs Spiked in Red Blood Cells (RBCs)

To determine the ability to discriminate between cell types, patient-derived, lung cancer dissociated tumor cells (LC-DTCs) were spiked in a solution of RBCs. Single LC-DTCs and RBCs flowing through the detection regions show unique electrical signatures and these signatures can be distinguished at flow-rates as high as 50 μL/min (Figure 3A, middle panel). Scatter plots (Figure 3A, right panel) show a representative sample of 50 single cells for each population and separation in the two populations using differential V_{pp} measurements.

C. Real-Time Impedance Measurement of DTCs Spiked in PBMCs

To assess the ability to distinguish between cancer cells and other blood cell types, LC-DTCs were spiked in a solution of patient-matched PBMCs (with no RBCs) and here too, distinct V_{pp} spectra (Figure 3B, middle panel) show that the cells can be distinguished in to two populations (Figure 4B, right panel) at flow rates as high as 50 μL/min.

D. Real-Time Impedance Measurement of LC-DTCs Spiked in Normal Cells

It is likely that tumor cell samples will contain healthy cell samples of the target organ, and to determine the ability to distinguish between the tumor cells and normal healthy cells we spiked LC-DTCs in normal lung cells. Specifically, adherent, fibroblast-like MRC-9 cells [7] were used as a normal lung cell control. While the V_{pp} spectra can show distinct differences, the scatter plots against $t_{transit}$ (Figure 3C, middle and right panel) show that normal lung and LC-DTCs can be distinguished but that care must be taken to ensure that only single cells are passing through the electrode regions as MRC-9 cells tend to clump and in cases confound the measurement.

E. Real-Time Impedance Measurement of DTCs Spiked in Normal Target-Organ Cells

To determine whether measurements as shown in Figure 4C are applicable to other cancer types, we spiked, thyroid, kidney, breast and ovarian cancer DTCs in their corresponding normal target cell counterparts. While thyroid, kidney and

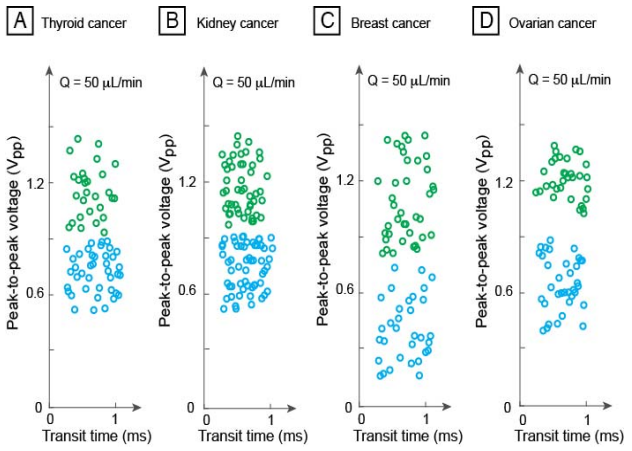

Fig. 4. *Real-time measurement of normal (blue) versus cancer (green) cell populations. Cancer cells are mixed with normal cells and are discriminated using peak-to-peak voltage measurements, n = 25 for each population. (A) and (B) show thyroid and kidney cancer, patient-derived cells, whereas (C) shows breast cancer cells which show greater spread in voltage and therefore size distributions. (D) Ovarian cancer cells are the most separable into different populations.*

ovarian samples (Figures 4A, B, and D) were separable at flow rates of 50 μL/min, breast cancer cells showed greater variation both in DTCs and normal cells. This could be attributed to culture conditions, since normal breast cells must be disrupted and dislodged from a growth surface prior to injection into the μEIS setup. Similarly, DTCs are thawed and re-suspended in growth medium, and the freeze thaw cycle could result in changes in cell morphologies for this particular sample.

IV. Discussion

Core biopsies have been the mainstays for diagnostic oncology but are limited in the ability to target certain organs or metastatic lesions. Liquid biopsies have garnered considerable interest for their capability to detect cancers with a routine blood test but necessarily require exquisite sensitivity for detecting either circulating tumor cells (CTCs) or circulating tumor DNA (ctDNA). Fine needle aspirates have the potential to provide clinically-relevant information directly from target organs by collecting small amounts of sample with a minimally-invasive technique. FNAs could also open the possibility to sampling metastatic lesions [8]. Given these unique capabilities, fine needle aspirates are showing increasing promise in clinical workflows. However, the inability to robustly collect sufficient sample has remained a hurdle. We have made a first step at addressing this hurdle by building a technological solution that can quickly (in a matter of minutes) analyze small volumes of patient-derived sample. This can provide reassurance that sufficient sample has been collected, enabling fewer collections to be performed, and can also provide assurance that the suspicious cells of interest (as opposed to cystic fluid or normal tissue) have been acquired.

Patient-derived samples such as DTCs serve as good analogs for tumor samples as they are derived from biopsies that are enzymatically and mechanically dissociated. Direct analysis of FNAs with our μEIS will require some form of further dissociation of cells either mechanically using ultrasonic agitation or enzymatically using reagents mixed into the sample streams, resulting in a single-cell suspension entering the electronic detection zones. While further manipulation of acquired FNAs will not preserve cell-cell associations and tissue architectures, the move toward genomic analysis of samples for diagnostic purposes where cell-cell interactions are necessarily disrupted bodes well for the adoption of our μEIS technique. While μEIS techniques have been employed in the past [8]–[10], none of these techniques, to our knowledge, has previously been employed to study fine needle aspirates. For future work, we aim to build a pipeline for acquisition of clinical samples to further validate the technology on acquired FNAs.

V. Conclusion

We have demonstrated that the μEIS can enumerate and discriminate cells, two of the major challenges for FNA analysis. Moreover, we have demonstrated this capability directly on patient-derived human samples and have distinguished cancer samples from target-organ-derived normal cells. In the long run, we envision that a μEIS system can be integrated into clinical workflows as an assistive device and even be directly integrated into tumor sampling needles.

Acknowledgments

The authors thank Dale Larson and Chris Salthouse for helpful technical discussions on coulter counters and electronic design; Dr. Thomas Ried, Dr. Gert Auer, and Dr. Miguel Sanchez for helpful discussions regarding the analysis of fine needle aspirate samples; and Amy Ly on the acquisition, staining and pathology workflows involved in FNAs. Special thanks to Heidi Perry, Sheila Hemami, and Kaigham Gabriel for supporting this work and our vision of using electronic signature analysis to improve health care.

References

[1] A. Ly, J. C. Ono, K. S. Hughes, M. B. Pitman, and R. Balassanian, "Fine-needle aspiration biopsy of palpable breast masses: Patterns of clinical use and patient experience," *J. Nat. Comprehensive Cancer Netw.*, vol. 14, no. 5, pp. 527–536, May 2016.

[2] I. D. Buley and D. E. Roskell, "Fine-needle aspiration cytology in tumour diagnosis: Uses and limitations," *Clin Oncol (R Coll Radiol)*, vol. 12, no. 3, pp. 71–166, 2000.

[3] H. Gharib and J. R. Goellner, "Fine-needle aspiration biopsy of the thyroid: An appraisal," *Ann. Internal Med.*, vol. 118, no. 4, pp. 282–289, Feb. 1993.

[4] V. Padmanabhan *et al.*, "Improving adequacy of small biopsy and fine-needle aspiration specimens for molecular testing by next-generation sequencing in patients with lung cancer," *Arch. Pathol. Lab. Med.*, vol. 14, no. 3, pp. 402–409, 2016.

[5] G. S. Gomez-Macias, R. Garza-Guajardo, J. Segura-Luna, and O. Barboza-Quintana, "Inadequate fine needle aspiration biopsy samples: Pathologists versus other specialists," *Cytojournal*, vol. 6, p. 9, Jun. 2009.

[6] Y. Xia and G. M. Whitesides, "Soft Lithography," *Annu. Rev. Mater. Sci.*, vol. 37, no. 5, pp. 550–575, 1998.

[7] J. P. Jacobs, A. J. Garrett, and R. Merton, "Characteristics of a serially propagated human diploid cell designated MRC-9," *J. Biol. Standardization*, vol. 7, no. 2, pp. 113–122, Apr. 1979.

[8] C. J. R. Stewart, J. Coldewey, and I. S. Stewart, "Comparison of fine needle aspiration cytology and needle core biopsy in the diagnosis of radiologically detected abdominal lesions," *J. Clin. Pathol.*, vol. 55, no. 2, pp. 93–97, Feb. 2002.

[9] K. Cheung, R. Gawad, and P. Renaud, "Impedance spectroscopy flow cytometry: On-chip label-free cell differentiation," *Cytometry Part A*, vol. 65, no. 2, pp. 124–132, Jun. 2005.

[10] R. Go'mez *et al.*, "Microfluidic biochip for impedance spectroscopy of biological species," *Biomed. Microdevices*, vol. 3, no. 3, pp. 201–209, Sep. 2001.